Preprints (www.preprints.org) | NOT PEER-REVIEWED | Posted: 21 September 2021 doi:10.20944/preprints202109.0361.v1

Article

Methodological investigation for hydrogen addition to small cage carbon fullerenes

Yuri Tanuma [1,2], Toru Maekawa[2,3] and Chris Ewels [1,*]

[1] Institut des Matériaux Jean Rouxel, CNRS / Université de Nantes, BP32229, 44322 Nantes, France; yuri.tanuma@cnrs-imn.fr
[2] Graduate School of Interdisciplinary New Science, Toyo University, 2100 Kujirai, Kawagoe, 350-8585, Saitama, Japan; s4r101900010@toyo.jp
[3] Bio-Nano Science Research Centre, Toyo University, 2100 Kujirai, Kawagoe, 350-8585, Saitama, Japan; maekawa@toyo.jp
* Correspondence: chris.ewels@cnrs-imn.fr; Tel.: +33 (0)2 40 37 64 07

Abstract: Hydrogenated small fullerenes (C_n, n<60) are of interest as potential astrochemical species, and as intermediates in hydrogen catalysed fullerene growth. However computational identification of key stable species is difficult due to the vast combinatorial space of structures. In this study we explore routes to predict stable hydrogenated small fullerenes. We show that neither local fullerene geometry nor local electronic structure analysis are able to correctly predict subsequent low energy hydrogenation sites, and indeed sequential stable addition searches also sometimes fail to identify most stable hydrogenated fullerene isomers. Of the empirical and semi-empirical methods tested, GFN2-xTB consistently gives highly accurate energy correlation (r>0.99) to full DFT-LDA calculations at a fraction of the computational cost. This allows identification of the most stable hydrogenated fullerenes up to 4H for four fullerenes, namely two isomers of C_{28} and C_{40}, via "brute force" systematic testing of all symmetry inequivalent combinations. The approach shows promise for wider systematic studies of smaller hydrogenated fullerenes.

Keywords: Fullerene; Hydrogenation; DFT; Functionalisation; Growth; xTB; REBO; Interstellar

1. Introduction

As well as in the laboratory and on earth, fullerenes have been found in a range of non-terrestrial environments [1–10]. Recent confirmation that C_{60}^+ is the source of some of the strong diffuse interstellar bands (DIBs) [5,11] suggests that fullerenes may play a key astrochemical role. However, the formation mechanisms of fullerenes in such extreme environments are still a debated question. Interestingly, while intuitively one might expect hydrogen to stabilise dangling bonds at edge sites and hence promote the formation of polyaromatic hydrocarbons rather than fullerenes, astrochemists have recently found that C_{60} and C_{70} are abundant in hydrogen-containing stars [8,9,12,13]. This suggests that hydrogen may play a role in fullerene growth. As such, stable hydrogenated small fullerenes are potentially of interest in astrochemistry, both as species in their own right and/or as degradation products from polyaromatic hydrocarbons [14], and as intermediates in the formation processes of larger fullerenes.

The stability of fullerenes strongly depends on the arrangement of pentagons and hexagons. According to the isolated pentagon rule (IPR), structures composed of isolated pentagons surrounded by five hexagons are favoured by the strain delocalisation and bonding [15]. The smallest fullerene to fully obey the IPR is the highly stable C_{60}, Buckminster fullerene. Fullerenes smaller than C_{60} are increasingly unstable due to steric strain originating within the non-IPR structures, and bond frustration in areas of high non-planarity. One route to potentially stabilise local strain and under-coordination is chemical functionalisation of the most reactive carbon sites. For example, experimental detection of

© 2021 by the author(s). Distributed under a Creative Commons CC BY license.

Preprints (www.preprints.org) | NOT PEER-REVIEWED | Posted: 21 September 2021 doi:10.20944/preprints202109.0361.v1

fullerane $C_{20}H_{20}$ [16] has been reported but not synthesis of pure C_{20}, and $C_{50}Cl_{10}$ has been isolated and characterised [17]. This suggests that relative stability of smaller fullerenes may be modified in the presence of hydrogen. While there has been extensive experimental [13,18–21] and theoretical [13,18,22] studies of hydrogenated C_{60}, less attention has been given to smaller hydrogenated fullerenes. It was theoretically proposed that T_d-$C_{28}H_4$, a tetrahedral fullerene with triply fused pentagons on each corner of the tetrahedron, might be stable [15], and indeed has since been experimentally identified [23]. For smaller fullerenes, an *in silico* investigation suggested fused-pentagon sites are preferred in general for single hydrogen addition [24].

Exploring the landscape of smaller hydrogenated fullerenes is potentially a highly complex and computationally intensive task. Very little can necessarily be determined in advance: neither the hydrogenation sites on the fullerene surface, nor the number of hydrogen additions – nor even the most stable carbon isomer for hydrogenation. This results in a vast and generally intractable number of potential calculations.

Considering first the number of pentagon and hexagon carbon fullerenes smaller than C_{60}, there is only 1 isomer for each of C_{20}, C_{24}, and C_{26}, and 2 for C_{28}. However, this rapidly increases, reaching 40 isomers for C_{40}, and 437 for C_{52}. In total there are 3958 C_x pentagon-hexagon fullerenes with x<60 [25].

Considering now hydrogenation, if symmetry is not taken into account then for a single fullerene C_n, there are n possible addition sites for a first hydrogen atom. However, this increases rapidly as more sites are hydrogenated. For two hydrogen atoms there are $n.(n\text{-}1)/2$ arrangements (divided by two since the hydrogens are interchangeable), and in general for m hydrogen atoms there are $n!/(n\text{-}m)!m!$ arrangements. Thus for $C_{28}H_5$ this gives 98,280 possible structures, and for larger hydrogenated species such as $C_{50}H_4$ there are 230,300 possibilities. While symmetry can help reduce these numbers, they remain highly challenging for standard density functional theory (DFT) calculations, where it can take several minutes on a state-of-the-art desktop PC to geometrically optimise even the smallest fullerene C_{20}. Since we do not in principle know how many hydrogen atoms are likely to bind to a given isomer, we would be required to start with single hydrogenation and then increase the number of hydrogen atoms sequentially until the hydrogen binding energy becomes too low.

Since the time cost for a brute force approach using DFT to this problem is not possible, it is the aim of the current study to explore, test and validate different possible methods that might be used to reduce the complexity of this problem and render it accessible computationally. This includes assumptions on growth sequence, use of geometric and electronic parameters as guides towards selecting the most reactive sites for functionalisation, and the use of different computational approximations such as empirical potentials and tight binding methods to increase calculation speed. We start with a sequence of DFT calculations, and use these thereafter as our benchmark energies for the subsequent studies.

2. Method

Coordinates for the fullerene cage structures are taken from Yoshida's fullerene library [26]. Geometric analysis of the fullerenes was performed using the *pychemcurv* python libraries discussed further in Ref [27].

All DFT calculations were carried out under the local density approximation (LDA) using the AIMPRO code [28–30]. Pseudo potentials are given by Hartwigsen, Goedecker, and Hutter (HGH) [31]. Wavefunctions are handled using a basis set of Gaussian type orbitals [32,33], in which 38 (12) independent functions are used for carbon (hydrogen) atoms. Charge density is handled using plane waves. Spin polarisation was used in systems with an odd or fractional number of electrons (μ_B=0.1,1,1.1) and averaged for systems

Preprints (www.preprints.org) | NOT PEER-REVIEWED | Posted: 21 September 2021 doi:10.20944/preprints202109.0361.v1

with an even number of electrons. Charged systems were handled by introducing a uniform homogenous compensating background charge to the cell. Electron temperature was handled using a Fermi function with temperature of 0.04eV to let the system be converged. All molecules were modelled in face-centred cells with a_0=15.875Å to ensure negligible inter-fullerene interactions. Structures were geometrically optimised until system energy was converged within 10^{-5} Ha, and positions to within 10^{-4} atomic units.

Empirical potential calculations are performed using the LAMMPS code [34], using the REBO [35], AIREBO [36] and AIREBO-M [37] potentials. In each case the structures are optimised with 10^{-10} convergence threshold (ratio of energy change to total energy magnitude), at zero Kelvin. The Reactive empirical bond order (REBO) is a potential developed by Brenner [35]. REBO is handled by a Tersoff-type potential [38,39], which deals with the formation and deformation of covalent bonds during a calculation and is developed for hydrogen [40] and carbon [40,41] containing systems. The Adaptive intermolecular reactive empirical bond order (AIREBO) potential [36] is developed for carbon-hydrogen systems. It uses REBO to describe nonbonded interactions. In this study, we included its torsion term and the Lennard-Jones (LJ) cutoff radius set at 2.5 (in σ scale factor). AIREBO-M is a hybrid potential of AIREBO and Morse [37]. In this potential, a LJ term in AIREBO is replaced with a Morse potential parameterised to Møller-Plesset method (MP2) calculations [42,43]. In this study, we included its torsion term and the Morse cutoff radius set at 3.0 (in σ scale factor).

Semi-empirical molecular orbital calculations were performed using MOPAC2016 [44] as implemented in the OpenMOPAC code. Default options were taken, except the MOZYME option which was selected, a method developed for quick calculations of organic molecules that replaces the self-consistent field (SCF) method with a localised molecular orbital (LMO) method. Different semi-empirical parameterisations were tested, namely PM6+D3, PM7 and RM1. PM6 [45] is fitted to reference data from DFT calculations, and here is combined with Grimme's D3 method for longer range dispersion interactions [46]. For PM7, geometric and enthalpy errors are improved compared to PM6 [45] by reconsidering new reference data [47]. In this method, D2 correlation is combined to take into account the dispersion. The correlation term is based on exchange-correlation functional of the generalised gradient approximation (GGA). Finally RM1 [48] is developed from AM1 [49] by improved parameters. It utilises different equations from PM6 to consider the core-core interactions.

Semi-empirical extended tight binding method (xTB) as implemented in GFN2-xTB is a quantum calculation method for gas and condensed phases developed by Grimme and co-workers [50]. It covers a large amount of elements up to radon, and is based on DFT perturbation expansion of the electron density, which makes it applicable to electronically complicated systems. For a huge number of isomers of fullerene C_{60}, xTB has already shown excellent structure-energy agreement with DFT results with Pearson's correlation coefficient r=0.998 [51]. Again we have used default settings including for convergence cutoffs.

3. Results

3.1 Pure Carbon Fullerenes

We first optimised using DFT-LDA all pure-carbon isomers of C_x fullerenes from x=20 to x=60. **Figure 1** shows on the y-axis the energy difference between a given isomer and the most stable isomer for the same number of carbon atoms. On the x-axis we give the number of atoms in the isomer neighbouring three pentagons. This plot confirms the general tendency that the stability of a given fullerene is negatively proportional to the number of triple fused pentagons, although there are a number of interesting exceptions.

Preprints (www.preprints.org) | NOT PEER-REVIEWED | Posted: 21 September 2021 doi:10.20944/preprints202109.0361.v1

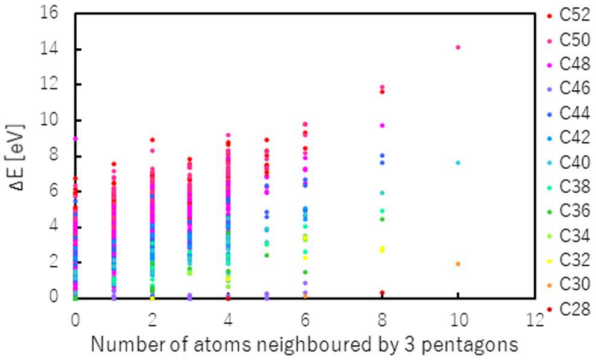

Figure 1. Plot of the number of atoms neighboured by triple pentagons versus energy difference compared to the ground state isomer. Structure instability is in general proportion to the number of triple pentagons. For optimal lowest energy isomer of C_x, $\Delta E=0$.

For the following hydrogenation study we focus on only four representative structures, C_{28} (1-T_d and 2-D_2, index of Yoshida's library[26]-symmetry symbol) and C_{40} (38-D_2 and 40-T_d) (see **Figure 2**). These are chosen since the T_d tetrahedral structures have 4, the maximum number, of triple fused pentagons and the other structures are the lowest energy pure-carbon structures in each isomer group.

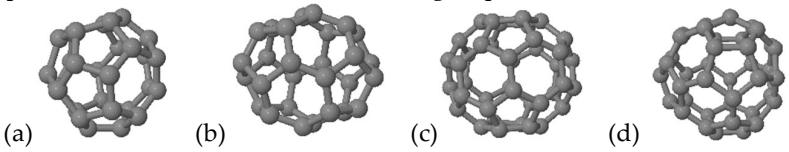

Figure 2. Structures for all site test. (a) C_{28} (1-T_d), (b) C_{28} (2-D_2), (c) C_{40} (38-D_2) and (d) C_{40} (40-T_d).

2.1. First hypothesis – sequential hydrogen addition.

In order to tackle the problem of the calculation time cost, our first hypothesis is that hydrogen atoms bind sequentially, in each case to the most stable site, and thereafter do not move. Such an approach was shown to successfully predict stable fluorinated fullerene [52], fullerene chlorination [53] and functionalisation with CF_3 groups [54,55]. This reduces the number of calculations substantially. To determine the stable structure of C_nH_m we first geometrically optimise the system C_nH with hydrogen in each of the n possible sites. We take the most stable solution and fixing the first hydrogen at this site, test the n-1 possible sites for the next hydrogen, and so on. As an example, for $C_{28}H_5$ this reduces the number of calculations from 98,280 to 130, and for $C_{50}H_4$ from 230,300 to 194, with the additional benefit that the stable structures for C_nH, C_nH_2, etc are automatically determined as part of the process.

While the method works well for halogens where the binding energies are high, its validity for hydrogenation is less clear. This hypothesis for sequential hydrogenation is tested in Sections 2.3 and 2.4 below. In the current section we employ sequential addition for our benchmark DFT calculations, exploring hydrogenation up to m=5, i.e. $C_{28}H_5$ and $C_{40}H_5$.

Preprints (www.preprints.org) | NOT PEER-REVIEWED | Posted: 21 September 2021 doi:10.20944/preprints202109.0361.v1

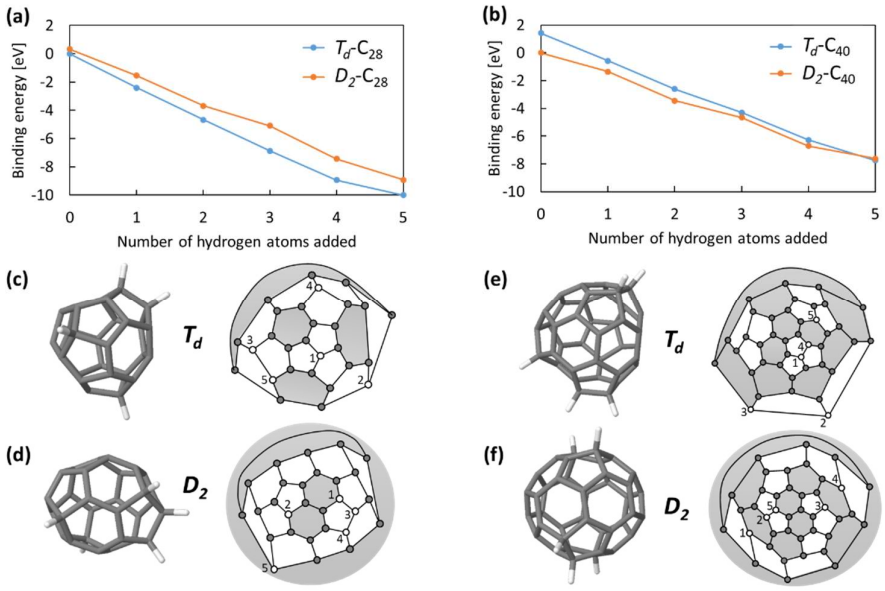

Figure 3. DFT-LDA Hydrogen binding energy relative to the most stable isomer and isolated H_2 (eV) for (a) C_{28} and (b) C_{40} obtained by sequential hydrogenation. T_d (D_2) isomer is given in blue (orange), symmetry notation refers to non-hydrogenated fullerene cage. (c-f) 3D molecular structures and Schlegel diagrams for C_nH_5. Grey and white represent carbon and hydrogenated carbon atoms, respectively. In the Schlegel diagrams, white circles indicate hydrogenated sites, hexagons are shaded grey. Numbering in Schlegel diagrams indicates the hydrogenation order.

Figure 3 shows the structures obtained this way for $C_{28}H_5$ and $C_{40}H_5$ for the two T_d and D_2 isomers. The energy axis shows the total binding energy of the hydrogen, calculated as

$$E_{binding} = E(C_nH_m) - E(C_n') - {}^m/_2\, E(H_2)$$

Where C_n is the fullerene in question and C_n' is the energetically most stable isomer fullerene. The projected Schlegel diagrams are marked numerically with the hydrogen addition sequence. T_d-C_{28} is sequentially hydrogenated at each triple pentagon on the tetrahedral corner sites, with the fifth hydrogenation occurring with lower binding energy visible as a change in the total energy gradient. At each stage this is the stable C_{28} isomer. In contrast, the stable C_{40} isomer is the lower symmetry D_2-C_{40}. Subsequent hydrogenation occurs around the "caps" of this isomer. However, hydrogen binds more strongly to the T_d-C_{40} isomer (although it does not this time adopt the triple pentagon tetrahedrally symmetric sites). This lowers the relative energy difference between the isomers until at $C_{40}H_5$ there is a transition and the T_d-$C_{40}H_5$ isomer becomes the most stable. This demonstrates that the most stable pure carbon isomer cannot be taken as a guide in general for which hydrogenated isomer will be stable, i.e. wider isomer testing is required.

2.2. Second hypothesis – predicting reactive sites via local geometry

The first hypothesis of sequential addition still requires every possible addition site to be geometrically optimised for each fullerene isomer, and it is desirable to reduce this further. In the section hypothesis, we postulate that the most reactive site for hydrogenation on a given fullerene might be determined in advance from the *local geometry of the fullerene before the hydrogen is added*. If this hypothesis is correct it allows prediction in advance of which site will be hydrogenated next, in principle reducing the number of calculations for $C_{28}H_5$ for example from 130 to simply 5.

There are a number of geometric parameters which have been explored in the literature as a way of indicating local site reactivity in fullerenes, most of which are discussed

Preprints (www.preprints.org) | NOT PEER-REVIEWED | Posted: 21 September 2021 doi:10.20944/preprints202109.0361.v1

in a good level of detail in Reference [27]. In general, they all try to quantify in some way the degree to which the p_z-orbital of the carbon atom is able to form a strong π-bond with one or more of its neighbours, typically through some measure of local curvature. In the following we select one geometric criterion and calculate its value for all non-hydrogenated sites on a given fullerene cage. The most extreme value (minimum or maximum, as discussed below) is taken as the next site to hydrogenate. The new structure is then geometrically optimised using DFT, and the process repeated. In this way a hydrogenation sequence is built up with geometric site selection at each step, and this sequence can be compared to the "lowest energy" sequence derived in Section 2.1.

We first tested pyramidalisation angle (PyrA). This is defined as θ-π/2 where θ is angle between the π-orbital axis vector (POAV) and a vector from a central atom to a side atom (except the atom along POAV) as shown in **Figure 4** [56–58]. The POAV is defined as a vector at constant angle to the three carbon-carbon bonds [59]. Thus in a flat graphene sheet the pyrA is zero. A further derivative from pyrA is the hybridisation value defined by Haddon [56–58] and explored further by Sabalot-Cuzzubbo and colleagues [11]. This is essentially a more chemical reworking of the pyrA in terms of the amount of $s^x p^y$ character in the system. For both of these parameters we calculated the values for all potential binding sites and selected the maximum for hydrogenation at each step.

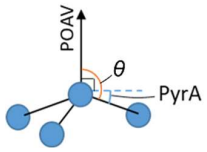

Figure 4. Schematic diagram of pyrA, defined as θ-π/2. POAV is the vector along the atom p_z orbital and is defined as having a constant angle with all three carbon-carbon bonds. Blue spheres represent carbon atoms.

An alternative geometric approach is to use bond lengths rather than angles. The idea behind this simple geometric test is that decreasing the π-bond character of an atom will tend to result in longer, purely single-character bonds, and hence a highly reactive radical should have three long single bonds. In the three-bond sum geometric parameter we simply sum the 3 bond lengths between a central atom and its adjacent atoms and hydrogenate the atom with the largest 3-bond sum. A refinement of the three-bond sum model is a two-bond sum. In principle in a strongly localised but non-aromatic π-bound atom it is possible to have 1 short double bond and 2 long single bonds in aromatic bonds, which may nonetheless result in a high three-bond sum. The two-bond sum model tries to avoid this by eliminating the shortest bond, and hydrogenating the atom with the lowest sum of the remaining two bond lengths.

In each of these four cases we followed the hydrogen addition sequence and compared the energy of the DFT-optimised structure with that found from testing all available sites at each addition step from Section 2.1 (**Figure 5**, Schlegel projections showing hydrogenation sites shown in **Figure S1**). As expected, hybridisation and pyrA give the same hydrogenation sequence. While these two parameters find the lowest energy structures for T_d-$C_{40}H$ and T_d-$C_{40}H_2$, in general none of these geometric methods correctly select the lowest energy hydrogenation sites, that is, none is capable of predicting the DFT predicted most stable structures.

Preprints (www.preprints.org) | NOT PEER-REVIEWED | Posted: 21 September 2021 doi:10.20944/preprints202109.0361.v1

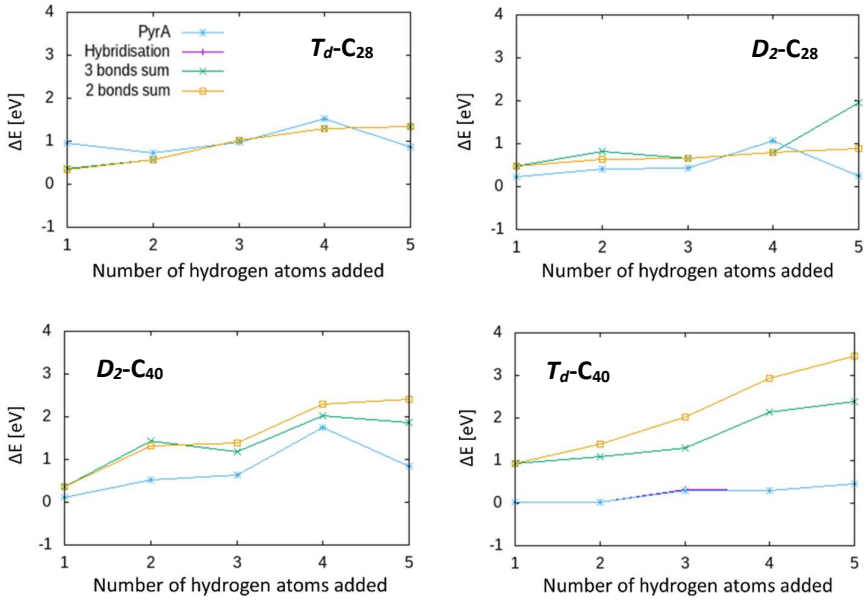

Figure 5. Plots of the difference in calculated total energy via DFT-LDA between hydrogenated fullerene structures, with hydrogen site selection based on geometric parameters (pyrA and hybridisation, and sum of two- or three- bond lengths), compared to the lowest energy hydrogenated isomer found through sequential addition from Section 2.1. Structures are C_{28} (1-*Td* and 2-D_2) and C_{40} (38-D_2 and 40-*Td*).

2.3. Third hypothesis - predicting reactive sites via local electronic structure.

Instead of using local geometry, we next considered potential hydrogenation site selection rules based on the local electronic structure of the parent molecule. It might be imagined that the site with the most local p_z-orbital character will release the most energy when hydrogenated. Alternatively, in cases where there is charge redistribution (notably on partially hydrogenated cages), sites showing excessive charging may also be targets for hydrogenation. We tested a number of electronic possibilities to select the next site for hydrogenation.

The simplest is to consider local Mulliken charges as determined by a Mulliken population analysis, as an estimate of atomic charge distribution in a molecule [60]. Hydrogenating the atom showing the highest Mulliken charge results in the sequence shown in **Figure 5** (blue trace, Schlegel projections in **Figure S1**), where clearly the lowest energy pathway is not selected. A more sophisticated approach is to use frontier orbitals [61]. In this case we add or remove some charge to the system, and by taking the difference in Mulliken values between the charged and neutral molecule, we identify where this charge is localising and can use that as indication of local site reactivity. Such an approach doubles the number of geometric optimisations required, since for each fullerene a second optimisation of the charged species is required, but this remains a tractable approach compared to the more "brute force" testing approaches described above. In essence adding some charge gives an indication of the localisation of the lowest unoccupied molecular orbital (LUMO), with the benefit of geometric optimisation allowing the system to respond to the charge state change.

In the following we tested two charging values, adding either 0.1*e* or a full electron to the system. Frontier orbital values for individual atoms were determined as the difference between the calculated Mulliken charge for the atom when the molecule was charged, and the Mulliken charge for that atom in the neutral system. Thus the lowest Frontier orbital value in the system indicates the atom that accumulates the most charge

Preprints (www.preprints.org) | NOT PEER-REVIEWED | Posted: 21 September 2021 doi:10.20944/preprints202109.0361.v1

when the 0.1/1*e* is added to the whole system, the highest Frontier orbital value is the atom that accumulates the least (or indeed loses the most charge if the frontier orbital value is positive). Once the site is chosen we hydrogenate this atom and continue with geometric optimisation in the neutral charge state as before. We tried following sequences of both the lowest, and highest frontier orbital values.

The results are shown in **Figure 6** (Schlegel projections in **Figure S1)**. In general, the frontier orbital values perform better than the simple Mulliken charges as a guide, and most give more stable isomers than the geometric parameters tested above. Nonetheless none of them are able to systematically reproduce the low energy structures obtained through sequential addition in Section 2.1. Thus we have demonstrated that the hypotheses of predicting hydrogenation sites on small fullerenes using the geometric and electronic parameters tested are not valid, i.e. these do not provide reliable routes to predicting hydrogenated structures directly from the parent fullerenes.

It is worth examining the Frontier orbital data for D_2-C_{28} in more detail, as it reveals another important result. It can be seen that when considering the lowest Frontier orbital atoms for hydrogenation, in the case of adding only 0.1*e*, for D_2-$C_{28}H_3$ and D_2-$C_{28}H_5$ the addition sequence actually predicts hydrogenated isomers that are *more stable* than those obtained in Section 2.1. This is important since it invalidates our first hypothesis, namely that sequential hydrogen addition always generates the lowest energy hydrogenated fullerenes. The implication is that if hydrogen can rearrange on the fullerene surface as further hydrogen atoms are added, this has the potential to lower the system energy. It is difficult to say whether kinetic barriers will limit this process in laboratory conditions; while calculations for single hydrogen migration suggest relatively high barriers [24], in practice a range of barriers will exist depending on local geometry, degree of hydrogen surface coverage, and local environment. In interstellar environments where UV-photon absorption is the primary interaction event [14], structural rearrangement is likely.

Thus we have demonstrated that none of the three proposed hypotheses provide a valid route to simplifying structure selection for hydrogenated fullerenes. This leaves a potentially intractable problem given the large number of hydrogenated fullerenes that need testing, and associated time for each DFT calculation. The next approach is therefore to try and reduce the computational cost of the calculations.

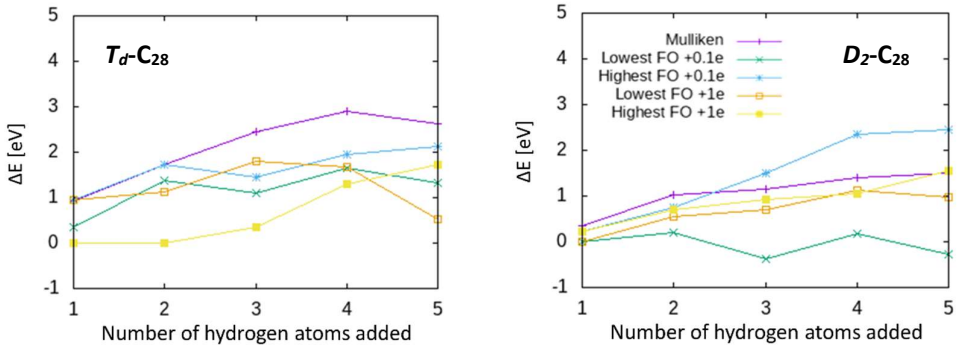

Preprints (www.preprints.org) | NOT PEER-REVIEWED | Posted: 21 September 2021 doi:10.20944/preprints202109.0361.v1

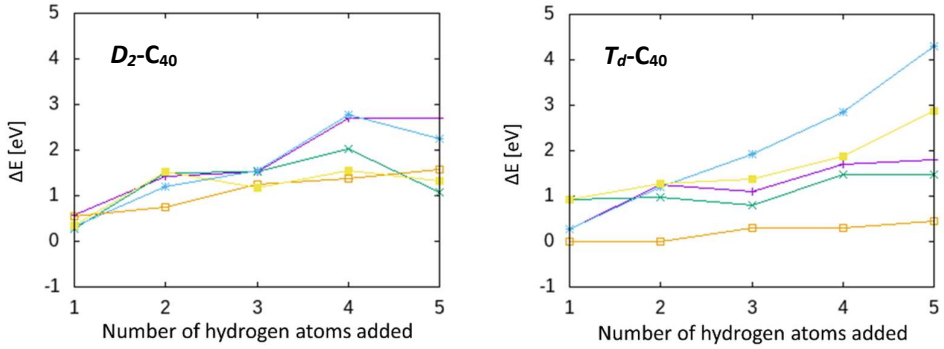

Figure 6. Plots of the difference in calculated total energy via DFT-LDA between hydrogenated fullerene structures, with hydrogenation sites selected based on the electronic parameters (Mulliken charges or Frontier orbital values) compared to the hydrogenated structures obtained in Section 2.1, for C_{28} (1-T_d and 2-D_2) and C_{40} (38-D_2 and 40-T_d).

2.4. Second strategy, semi-empirical and empirical routes

Rather than applying selection rules to simplify the problem and then using high level, but slow, DFT tools, an alternative approach is to not simplify the problem but instead tackle every possible hydrogenated fullerene, and simplify instead the tool used to make the calculation time acceptable. We use our extensive collection of DFT calculations from Section 2.1 as a comparative benchmark. We test the four representative structures using the following methods: Empirical potentials using LAMMPS [34], Semi-empirical molecular orbital approaches using MOPAC [44], and a relatively new semi-empirical extended tight binding method (GFN2-xTB). GFN2-xTB has previously shown excellent structure-energy agreement with DFT results for C_{60} isomers, with Pearson's correlation coefficient r=0.998 [51].

In each case we have geometrically optimised the structure using the method described, and then plotted the calculated total energy against that calculated using DFT-LDA. The results are shown for $C_{40}H_5$ in **Figure 7**, along with the corresponding Pearson's correlation coefficient. Plots for two other fullerenes ($C_{28}H_5$ and $C_{40}H$) are shown in **Figure S1, S2**.

The empirical potential-based methods (REBO, AIREBO and AIREBO-M) show essentially no correlation (r<0.4) with the DFT-LDA energies. In contrast the MOPAC semi-empirical based methods show the same overall energetic stability tendency as DFT, with correlation in the range r=0.75~0.77. All three methods show very similar distribution of points. However, in the all three cases the most stable structure by DFT does not correspond to that obtained by the semi-empirical methods, and indeed lies someway off (for $C_{40}H_5$, using PM7, PM6+D3 and RM1 the structure predicted by DFT-LDA to be the most stable structure is only 20th on a list of 72). Thus even if these methods were used to prescreen suitable structures and a cut-off applied (with full DFT-LDA geometric optimisation of only the most stable RM1 structures), the cut-off would necessarily have to be quite high, at least 30% of structures, in order to ensure that the lowest energy DFT-LDA structure was included.

In strong contrast to the above methods, GFN2-xTB shows outstandingly good correlation (r=0.98) in energetic stability compared to DFT-LDA. Enlarging the lowest energy range, there is a data cluster and the lowest energy structure in DFT shows the lowest energy also by the GFN2-xTB calculation isolated from the other close data points. For other simpler fullerenes (less hydrogenated and a smaller cage) the correlation is even better (**Figure S1**, **S2**), r=0.993-0.998.

Preprints (www.preprints.org) | NOT PEER-REVIEWED | Posted: 21 September 2021 doi:10.20944/preprints202109.0361.v1

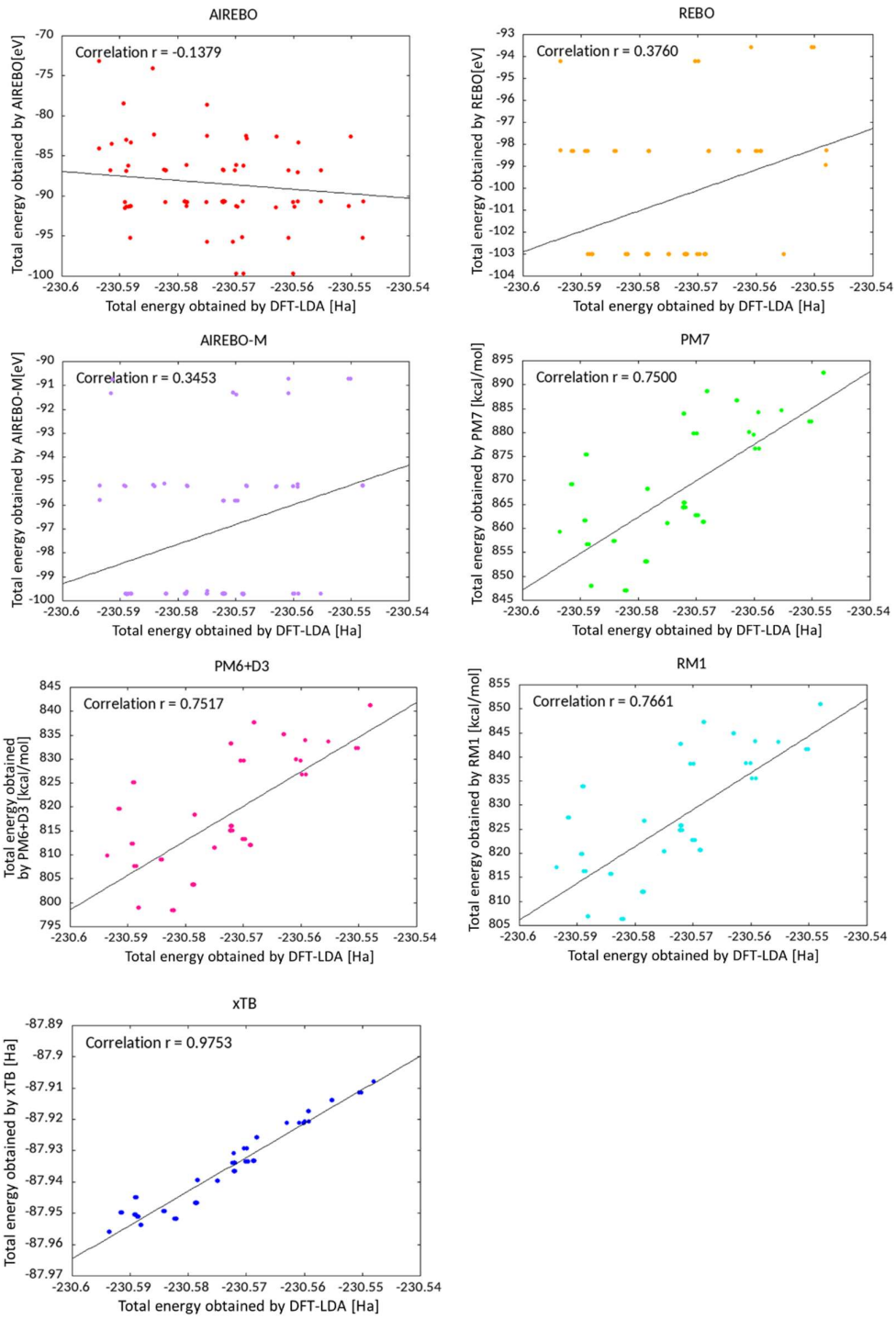

Figure 7. Total energy correlation plots for isomers of $C_{40}H_5$. Energy obtained by DFT-LDA is plotted along the x-axis and by empirical and semi-empirical methods along the y-axes as labelled. Linear correlation in each model is shown as r in each plot.

If we compare calculation times for these different methods, the potential advantages are clear. The average run-time of each calculation for pure C_{20} on a 16-core desktop PC is summarised in **Table 1** (along with the corresponding r-values from **Figure 7**). As expected the empirical potentials are the fastest but show no correlation to the DFT-LDA total energies. Of the semi-empirical methods GFN2-xTB shows by far the best run time, as well as giving the best correlation to DFT-LDA. These results show that we can safely

Preprints (www.preprints.org) | NOT PEER-REVIEWED | Posted: 21 September 2021 doi:10.20944/preprints202109.0361.v1

switch to using GFN2-xTB, since it is able to successfully generate DFT-LDA accuracy in total energies of hydrogenated smaller fullerenes, but at over 600 times less computational time.

Table 1. Comparison of empirical and semi-empirical methods with DFT. Run time is the average of 10 runs for pure C_{20}. r is Pearson's correlation coefficient from **Figure 7**.

Method	AIREBO	REBO	AIREBO-M	PM7	PM6+D3	RM1	xTB	DFT
Run time	0.039 s	0.039 s	0.043 s	1.33 s	0.95 s	0.91 s	0.34 s	210 s
r	-0.1379	0.3760	0.3453	0.7500	0.7517	0.7661	0.9753	-

2.5. All combination of hydrogenation sites testing by xTB

Next we tested all the possible combination of hydrogenation sites up to 4th hydrogenation using GFN2-xTB for the four fullerene structures discussed above, T_d-C_{28}, D_2-C_{28}, T_d-C_{40} and D_2-C_{40}. This brute force approach calculates the total energy for all hydrogen isomers of fullerenes C_nH_m, unlike the sequential test described in Section 2.1. As such it provides a definitive lowest energy hydrogenation sequence for C_nH_m, m=0…4.

For $C_{28}H_4$, the most stable structure found is the T_d-$C_{28}H_4$ shown in **Figure 8** (Schlegel projection shown in Figure S1). This has tetrahedral symmetry, and corresponds to the structure found in the literature [23]. This is also the most stable structure found through sequential addition (using DFT-LDA, GFN2-xTB, PM7, PM6+D3 and RM1). Energies of all the possible isomers are summarised in **Figure 8**. The single data point at the lowest energy lies significantly below the others, i.e. for $C_{28}H_4$ there is a single stable hydrogenated structure. The D_2-C_{28} isomer is significantly less stable; within the D_2-$C_{28}H_4$ subset of results, the most stable isomer consists of two hydrogen pairs at opposing ends of the molecule. This can be understood in terms of a localisation of strain, allowing a maximum flattening out and aromaticity in the two hexagon pairs along the fullerene sides. This structure is different, and more stable, than that found for D_2-$C_{28}H_4$ by sequential addition in Section 2.1 above.

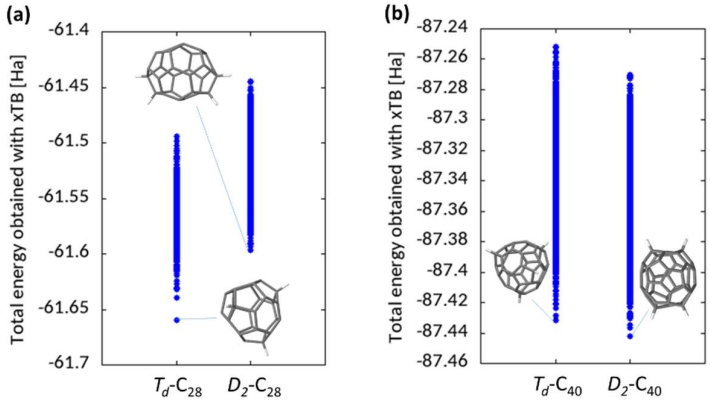

Figure 8. Calculated total energy of all the possible (a) $C_{28}H_4$ and (b) $C_{40}H_4$ for T_d and D_2 isomers obtained by GFN2-xTB, with lowest energy structures labelled.

The lowest energy C_nH_m structures for H=1…4 for the two isomers are shown in **Figure 9**. The T_d sequence for C_{28} is largely sequential functionalisation of the triple pentagons, the exception being $C_{28}H_3$. In this case the sequential structure has only a single unfunctionalised triple pentagon which means the radical is highly localised, and hence it is more stable to redistribute the hydrogen atoms. In contrast the D_2-C_{28} lowest energy series is not at all sequential, with different hydrogenation combinations balancing relief of localised

Preprints (www.preprints.org) | NOT PEER-REVIEWED | Posted: 21 September 2021 doi:10.20944/preprints202109.0361.v1

curvature at the fullerene "ends" with radical redistribution. This flux of different structures is also presumably indicative of the relative instability of this isomer compared to the T_d.

The situation with C_{40} is somewhat different. In this case the most stable structures match exactly the series found through sequential addition in Section 2.1. For the T_d-isomer this is presumably because in this case the curvature at the triple pentagon is less localised than in C_{28} due to the larger cage size, allowing more delocalisation of the radical for $C_{40}H_3$. For the D_2 isomer hydrogenation localises the curvature at the fullerene ends resulting in a cylindrical structure somewhat resembling a small diameter capped carbon nanotube. The D_2 isomer is the most stable for all species up to $C_{40}H_4$. The relative energies show that hydrogenation is increasingly stabilising the T_d isomer (and indeed as shown above, at $C_{40}H_5$ there is an inversion in stability and the T_d is more favoured). Further testing will be needed to determine whether, in larger fullerenes such as C_{40} and above, the lowest energy hydrogenated fullerenes always match the sequential addition patterns. If so, this would represent a significant computational benefit.

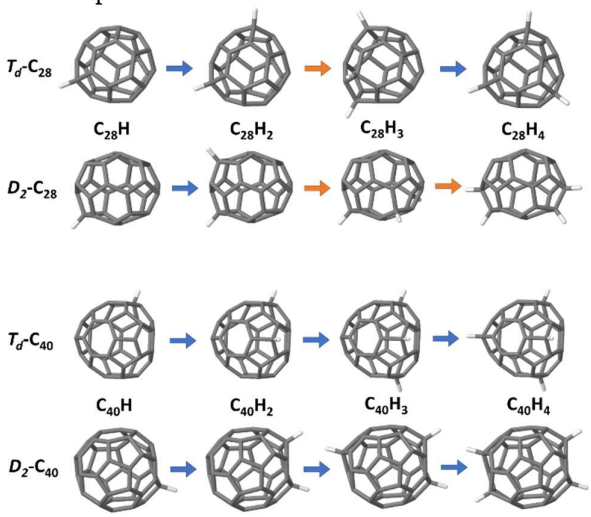

Figure 9. The lowest energy C_nH_m structures for n=28 and 40, and m=1…4 for the T_d and D_2 isomers calculated using GFN2-xTB testing all symmetry inequivalent possibilities. Grey and white in molecular structures represent carbon and hydrogen atoms. Blue arrow indicates hydrogenation in a sequential route, while orange arrow indicates non-sequential hydrogenation.

4. Discussion

This study draws out several key points when designing a methodology to explore the vast configurational space of hydrogenated isomers of small fullerenes.

The first is that unfortunately it does not appear possible to systematically predict subsequent lowest energy hydrogenation sites based on either the geometry or electronic structure of a given fullerene or hydrogenated fullerene, at least not with the parameters that we have tested here. There are a number of potential reasons for this, including substantial strain relaxation of the structure, and charge and aromaticity redistribution after hydrogenation.

It has also been demonstrated that the hypothesis that hydrogen atoms are added sequentially and do not then move does not always result in the lowest energy hydrogenated fullerene isomer for multiple hydrogenation events. Nonetheless this procedure generates quite low energy pathways and in many cases effectively did identify the lowest energy isomers. It may be possible to use a modified version of this procedure (for example allowing hydrogen atoms a limited number of site changes to neighbouring sites before subsequent hydrogen addition) in order to improve the robustness of the algorithm while maintaining a tractable number of structures to explore. Additionally, in laboratory hydrogenation conditions where kinetic barriers for surface migration may be difficult to

Preprints (www.preprints.org) | NOT PEER-REVIEWED | Posted: 21 September 2021 doi:10.20944/preprints202109.0361.v1

overcome, this hypothesis may still result in predicting experimentally detectable isomers, which may not necessarily be those with the lowest total energy.

Considering both the calculation costs and the correlation to full DFT-LDA results, GFN2-xTB appears to give reliable and rapid results for hydrogenation of small fullerenes. The predictability is supposed to originate with the DFT-based parameters for the electron density in the reference data.

In the case of C_{28}, the lowest energy hydrogenated structure is T_d-$C_{28}H_4$ with tetrahedral hydrogenation; each triple pentagon is hydrogenated. This relaxes the angle strain localised on the tetrahedral corners and is consistent with literature observations. For the D_2-C_{28} isomer there are two six-fused pentagons along its sides, and curvature localised at the caps is partially relieved by pairwise hydrogenation at each cap. Nonetheless the four hydrogen atoms appear insufficient to relax it and the structure is much less stable than the tetrahedral solution.

In contrast, in the case of C_{40}, the T_d isomer is less stable then the D_2 isomer. Instead, the D_2 isomer, in which there are no triple fused pentagon but 2 six-pentagon chains, shows the lowest energy. When we look at the structure of $C_{40}H_4$, indeed fused pentagon (pentagon chains) sites are hydrogenated [3], not only on the triple pentagons. We suppose that for the larger fullerene cages pentagon chain structures may play an important role to stabilise the whole structure of non-IPR species.

Given the rapidity and accuracy of the approach using GFN2-xTB, it is now our intention to pursue the most stable C_nH_m structures for other small fullerenes, with the eventual intention of mapping hydrogen catalysed fullerene growth.

Supplementary Materials: The following are available online at www.mdpi.com/xxx/s1, Figure S1: title.

Author Contributions: Conceptualisation, C.E.; methodology, C.E. and Y.T.; validation, C.E., T.M.; investigation, Y.T.; resources, C.E.; data curation, Y.T., C.E.; writing—original draft preparation, Y.T., C.E.; writing—review and editing, T.M., C.E.; supervision, T.M., C.E.; project administration, T.M., C.E.; funding acquisition, T.M., Y.T., C.E. All authors have read and agreed to the published version of the manuscript.

Funding: This research was funded by Inoue Enryo Memorial Grant of Toyo University and Y.T. acknowledges financial support from French governmental bursary JP19-00207. Computing support was funded by Region Pays de la Loire "Paris Scientifiques 2017", Grant Number 09375.

Informed Consent Statement: Not applicable.

Data Availability Statement: Please refer to suggested Data Availability Statements in section "MDPI Research Data Policies" at https://www.mdpi.com/ethics.

Conflicts of Interest: The authors declare no conflict of interest.

References

1. García-Hernández, D.A.; Manchado, A.; García-Lario, P.; Stanghellini, L.; Villaver, E.; Shaw, R.A.; Szczerba, R.; Perea-Calderón, J.V. Formation of Fullerenes in H-Containing Planetary Nebulae. *Astrophysical Journal Letters* **2010**, doi:10.1088/2041-8205/724/1/L39.
2. García-Hernndez, D.A.; Iglesias-Groth, S.; Acosta-Pulido, J.A.; Manchado, A.; García-Lario, P.; Stanghellini, L.; Villaver, E.; Shaw, R.A.; Cataldo, F. The Formation of Fullerenes: Clues from New C60, C70, and (Possible) Planar C24 Detections in Magellanic Cloud Planetary Nebulae. *Astrophysical Journal Letters* **2011**, doi:10.1088/2041-8205/737/2/L30.
3. Bernard-Salas, J.; Cami, J.; Peeters, E.; Jones, A.P.; Micelotta, E.R.; Groenewegen, M.A.T. ON THE EXCITATION AND FORMATION OF CIRCUMSTELLAR FULLERENES. *ApJ* **2012**, *757*, 41, doi:10.1088/0004-637X/757/1/41.
4. Otsuka, M.; Kemper, F.; Cami, J.; Peeters, E.; Bernard-Salas, J. Physical Properties of Fullerene-Containing Galactic Planetary Nebulae. *Monthly Notices of the Royal Astronomical Society* **2014**, *437*, 2577–2593, doi:10.1093/mnras/stt2070.
5. Campbell, E.K.; Holz, M.; Gerlich, D.; Maier, J.P. Laboratory Confirmation of C60(+) as the Carrier of Two Diffuse Interstellar Bands. *Nature* **2015**, *523*, 322–323, doi:10.1038/nature14566.
6. Sellgren, K.; Werner, M.W.; Ingalls, J.G.; Smith, J.D.T.; Carleton, T.M.; Joblin, C. C60 in Reflection Nebulae. *Astrophysical Journal Letters* **2010**, doi:10.1088/2041-8205/722/1/L54.

Preprints (www.preprints.org) | NOT PEER-REVIEWED | Posted: 21 September 2021 doi:10.20944/preprints202109.0361.v1

7. Berné, O.; Cox, N.L.J.; Mulas, G.; Joblin, C. Detection of Buckminsterfullerene Emission in the Diffuse Interstellar Medium. *Astron Astrophys* **2017**, *605*, L1, doi:10.1051/0004-6361/201630325.
8. Berné, O.; Tielens, A.G.G.M. Formation of Buckminsterfullerene (C60) in Interstellar Space. *PNAS* **2012**, *109*, 401–406, doi:10.1073/pnas.1114207108.
9. Candian, A.; Gomes Rachid, M.; MacIsaac, H.; Staroverov, V.N.; Peeters, E.; Cami, J. Searching for Stable Fullerenes in Space with Computational Chemistry. *Monthly Notices of the Royal Astronomical Society* **2019**, *485*, 1137–1146, doi:10.1093/mnras/stz450.
10. Clayton, G.C.; Marco, O.D.; Whitney, B.A.; Babler, B.; Gallagher, J.S.; Nordhaus, J.; Speck, A.K.; Wolff, M.J.; Freeman, W.R.; Camp, K.A.; et al. THE DUST PROPERTIES OF TWO HOT R CORONAE BOREALIS STARS AND A WOLF-RAYET CENTRAL STAR OF A PLANETARY NEBULA: IN SEARCH OF A POSSIBLE LINK. *AJ* **2011**, *142*, 54, doi:10.1088/0004-6256/142/2/54.
11. Foing, B.H.; Ehrenfreund, P. Detection of Two Interstellar Absorption Bands Coincident with Spectral Features of C60+. *Nature* **1994**, *369*, 296–298, doi:10.1038/369296a0.
12. García-Hernndez, D.A.; Rao, N.K.; Lambert, D.L. Are C60 Molecules Detectable in Circumstellar Shells of R Coronae Borealis Stars? *Astrophysical Journal* **2011**, doi:10.1088/0004-637X/729/2/126.
13. Palotás, J.; Martens, J.; Berden, G.; Oomens, J. The Infrared Spectrum of Protonated Buckminsterfullerene C60H+. *Nat Astron* **2020**, *4*, 240–245, doi:10.1038/s41550-019-0941-6.
14. Omont, A.; Bettinger, H.F. Intermediate-Size Fullerenes as Degradation Products of Interstellar Polycyclic Aromatic Hydrocarbons. *A&A* **2021**, *650*, A193, doi:10.1051/0004-6361/202140675.
15. Kroto, H.W. The Stability of the Fullerenes C n , with n = 24, 28, 32, 36, 50, 60 and 70. *Nature* **1987**, *329*, 529–531, doi:10.1038/329529a0.
16. Prinzbach, H.; Weiler, A.; Landenberger, P.; Wahl, F.; Wörth, J.; Scott, L.T.; Gelmont, M.; Olevano, D.; Issendorff, B. v Gas-Phase Production and Photoelectron Spectroscopy of the Smallest Fullerene, C 20. *Nature* **2000**, *407*, 60–63, doi:10.1038/35024037.
17. Xie, S.-Y.; Gao, F.; Lu, X.; Huang, R.-B.; Wang, C.-R.; Zhang, X.; Liu, M.-L.; Deng, S.-L.; Zheng, L.-S. Capturing the Labile Fullerene[50] as C50Cl10. *Science* **2004**, *304*, 699–699, doi:10.1126/science.1095567.
18. Hall, L.E.; McKenzie, D.R.; Attalla, M.I.; Vassallo, A.M.; Davis, R.L.; Dunlop, J.B.; Cockayne, D.J.H. The Structure of Hydrogenated Fullerene (C60H36). *J. Phys. Chem.* **1993**, *97*, 5741–5744, doi:10.1021/j100123a046.
19. Cataldo, F. Fullerane, the Hydrogenated C60 Fullerene: Properties and Astrochemical Considerations. *Fullerenes, Nanotubes and Carbon Nanostructures* **2003**, *11*, 295–316, doi:10.1081/FST-120025852.
20. Iglesias-Groth, S.; García-Hernández, D.A.; Cataldo, F.; Manchado, A. Infrared Spectroscopy of Hydrogenated Fullerenes (Fulleranes) at Extreme Temperatures: *Hydrogenated Fullerenes at Extreme Temperatures*. *Monthly Notices of the Royal Astronomical Society* **2012**, *423*, 2868–2878, doi:10.1111/j.1365-2966.2012.21097.x.
21. Goldshleger, N.F.; Moravsky, A.P. Fullerene Hydrides: Synthesis, Properties, and Structure. *Russ. Chem. Rev.* **1997**, *66*, 323, doi:10.1070/RC1997v066n04ABEH000291.
22. Zhang, Y.; Sadjadi, S.; Hsia, C.-H.; Kwok, S. Search for Hydrogenated C60(Fulleranes) in Circumstellar Envelopes. *ApJ* **2017**, *845*, 76, doi:10.3847/1538-4357/aa71ac.
23. Veljković, M.; Nešković, O.; Djerić, A.; Veličković, S.; Šipka, V. Hypervalent Molecular Cluster: C28H4. *Materials Science Forum* **2005**, *494*, 181–186, doi:10.4028/www.scientific.net/MSF.494.181.
24. EL-Barbary, A.A. Hydrogenation Mechanism of Small Fullerene Cages. *International Journal of Hydrogen Energy* **2016**, *41*, 375–383, doi:10.1016/j.ijhydene.2015.10.102.
25. Fowler, P.W.; Manolopoulos, D.E. *An Atlas of Fullerenes*; Clarendon Press: Oxford, 1995; ISBN 0-19-855787-6.
26. Yoshida, M. Yoshida's Fullerene Library Available online: http://www.jcrystal.com/steffenweber/gallery/Fullerenes/Fullerenes.html (accessed on 18 November 2020).
27. Sabalot-Cuzzubbo, J.; Salvato-Vallverdu, G.; Bégué, D.; Cresson, J. Relating the Molecular Topology and Local Geometry: Haddon's Pyramidalisation Angle and the Gaussian Curvature. *J. Chem. Phys.* **2020**, *152*, 244310, doi:10.1063/5.0008368.
28. Rayson, M.J.; Briddon, P.R. Highly Efficient Method for Kohn-Sham Density Functional Calculations of 500-10000 Atom Systems. *Physical Review B - Condensed Matter and Materials Physics* **2009**, doi:10.1103/PhysRevB.80.205104.
29. Rayson, M.J. Rapid Filtration Algorithm to Construct a Minimal Basis on the Fly from a Primitive Gaussian Basis. *Computer Physics Communications* **2010**, doi:10.1016/j.cpc.2010.02.012.
30. Briddon, P.R.; Rayson, M.J. Accurate Kohn–Sham DFT with the Speed of Tight Binding: Current Techniques and Future Directions in Materials Modelling. *physica status solidi (b)* **2011**, *248*, 1309–1318, doi:https://doi.org/10.1002/pssb.201046147.
31. Hartwigsen, C.; Goedecker, S.; Hutter, J. Relativistic Separable Dual-Space Gaussian Pseudopotentials from H to Rn. *Phys. Rev. B* **1998**, *58*, 3641–3662, doi:10.1103/PhysRevB.58.3641.
32. Kohn, W.; Sham, L.J. Self-Consistent Equations Including Exchange and Correlation Effects. *Physical Review* **1965**, doi:10.1103/PhysRev.140.A1133.
33. Briddon, P.R.; Jones, R. LDA Calculations Using a Basis of Gaussian Orbitals. *physica status solidi (b)* **2000**, *217*, 131–171, doi:https://doi.org/10.1002/(SICI)1521-3951(200001)217:1<131::AID-PSSB131>3.0.CO;2-M.
34. Plimpton, S. Fast Parallel Algorithms for Short-Range Molecular Dynamics. *Journal of Computational Physics* **1995**, *117*, 1–19, doi:10.1006/jcph.1995.1039.
35. Brenner, D.W.; Shenderova, O.A.; Harrison, J.A.; Stuart, S.J.; Ni, B.; Sinnott, S.B. A Second-Generation Reactive Empirical Bond Order (REBO) Potential Energy Expression for Hydrocarbons. *J. Phys.: Condens. Matter* **2002**, *14*, 783–802, doi:10.1088/0953-8984/14/4/312.

Preprints (www.preprints.org) | NOT PEER-REVIEWED | Posted: 21 September 2021 doi:10.20944/preprints202109.0361.v1

36. Stuart, S.J.; Tutein, A.B.; Harrison, J.A. A Reactive Potential for Hydrocarbons with Intermolecular Interactions. *J. Chem. Phys.* **2000**, *112*, 6472–6486, doi:10.1063/1.481208.
37. O'Connor, T.C.; Andzelm, J.; Robbins, M.O. AIREBO-M: A Reactive Model for Hydrocarbons at Extreme Pressures. *J. Chem. Phys.* **2015**, *142*, 024903, doi:10.1063/1.4905549.
38. Tersoff, J. New Empirical Approach for the Structure and Energy of Covalent Systems. *Phys. Rev. B* **1988**, *37*, 6991–7000, doi:10.1103/PhysRevB.37.6991.
39. Tersoff, J. Modeling Solid-State Chemistry: Interatomic Potentials for Multicomponent Systems. *Phys. Rev. B* **1989**, *39*, 5566–5568, doi:10.1103/PhysRevB.39.5566.
40. Brenner, D.W. Tersoff-Type Potentials for Carbon, Hydrogen and Oxygen. *MRS Online Proceedings Library (OPL)* **1988**, *141*, doi:10.1557/PROC-141-59.
41. Tersoff, J. Empirical Interatomic Potential for Carbon, with Applications to Amorphous Carbon. *Phys. Rev. Lett.* **1988**, *61*, 2879–2882, doi:10.1103/PhysRevLett.61.2879.
42. Møller, Chr.; Plesset, M.S. Note on an Approximation Treatment for Many-Electron Systems. *Phys. Rev.* **1934**, *46*, 618–622, doi:10.1103/PhysRev.46.618.
43. Dunning, T.H. Gaussian Basis Sets for Use in Correlated Molecular Calculations. I. The Atoms Boron through Neon and Hydrogen. *J. Chem. Phys.* **1989**, *90*, 1007–1023, doi:10.1063/1.456153.
44. Stewart, J.J.P. *MOPAC2016*; Stewart Computational Chemistry, Colorado Springs: CO, USA;
45. Stewart, J.J.P. Optimization of Parameters for Semiempirical Methods V: Modification of NDDO Approximations and Application to 70 Elements. *J Mol Model* **2007**, *13*, 1173–1213, doi:10.1007/s00894-007-0233-4.
46. Grimme, S.; Antony, J.; Ehrlich, S.; Krieg, H. A Consistent and Accurate Ab Initio Parametrization of Density Functional Dispersion Correction (DFT-D) for the 94 Elements H-Pu. *J. Chem. Phys.* **2010**, *132*, 154104, doi:10.1063/1.3382344.
47. Stewart, J.J.P. Optimization of Parameters for Semiempirical Methods VI: More Modifications to the NDDO Approximations and Re-Optimization of Parameters. *J Mol Model* **2013**, *19*, 1–32, doi:10.1007/s00894-012-1667-x.
48. Rocha, G.B.; Freire, R.O.; Simas, A.M.; Stewart, J.J.P. RM1: A Reparameterization of AM1 for H, C, N, O, P, S, F, Cl, Br, and I. *Journal of Computational Chemistry* **2006**, *27*, 1101–1111, doi:10.1002/jcc.20425.
49. Dewar, M.J.S.; Zoebisch, E.G.; Healy, E.F.; Stewart, J.J.P. Development and Use of Quantum Mechanical Molecular Models. 76. AM1: A New General Purpose Quantum Mechanical Molecular Model. *J. Am. Chem. Soc.* **1985**, *107*, 3902–3909, doi:10.1021/ja00299a024.
50. Bannwarth, C.; Caldeweyher, E.; Ehlert, S.; Hansen, A.; Pracht, P.; Seibert, J.; Spicher, S.; Grimme, S. Extended Tight-Binding Quantum Chemistry Methods. *WIREs Computational Molecular Science* **2021**, *11*, e1493, doi:10.1002/wcms.1493.
51. Sure, R.; Hansen, A.; Schwerdtfeger, P.; Grimme, S. Comprehensive Theoretical Study of All 1812 C60 Isomers. *Phys. Chem. Chem. Phys.* **2017**, *19*, 14296–14305, doi:10.1039/C7CP00735C.
52. Van Lier, G.; Cases, M.; Ewels, C.P.; Taylor, R.; Geerlings, P. Theoretical Study of the Addition Patterns of C60 Fluorination: C60Fn (n = 1–60). *J. Org. Chem.* **2005**, *70*, 1565–1579, doi:10.1021/jo0483872.
53. Vlandas, A.; Ewels, C.P.; Lier, G.V. Controlling Fullerene Addition Sequences, Regioselectivity and Magic Numbers via Metal Encapsulation. *Chem. Commun.* **2011**, *47*, 7051–7053, doi:10.1039/C1CC11072A.
54. Nakagawa, A.; Nishino, M.; Niwa, H.; Ishino, K.; Wang, Z.; Omachi, H.; Furukawa, K.; Yamaguchi, T.; Kato, T.; Bandow, S.; et al. Crystalline Functionalized Endohedral C60 Metallofullerides. *Nat Commun* **2018**, *9*, 3073, doi:10.1038/s41467-018-05496-8.
55. Ewels, C.; Rio, J.; Niwa, H.; Omachi, H.; Shinohara, H.; Rayson, M.; Briddon, P. Determining Addition Pathways and Stable Isomers for CF3 Functionalisation of Endohedral Gd@C60. *Royal Society Open Science* **2018**, *5*, 180588, doi:10.1098/rsos.180588.
56. Haddon, R.C. C_{60} : Sphere or Polyhedron? *J. Am. Chem. Soc.* **1997**, *119*, 1797–1798, doi:10.1021/ja9637659.
57. Haddon, R.C.; Scott, L.T. π-Orbital conjugation and rehybridization in bridged annulenes and deformed molecules in general: π-orbital axis vector analysis. *Pure and Applied Chemistry* **1986**, *58*, 137–142, doi:10.1351/pac198658010137.
58. Haddon, R.C. Hybridization and the Orientation and Alignment of .Pi.-Orbitals in Nonplanar Conjugated Organic Molecules: .Pi.-Orbital Axis Vector Analysis (POAV2). *J. Am. Chem. Soc.* **1986**, *108*, 2837–2842, doi:10.1021/ja00271a009.
59. Haddon, R.C. Comment on the Relationship of the Pyramidalisation Angle at a Conjugated Carbon Atom to the σ Bond Angles. *J. Phys. Chem. A* **2001**, *105*, 4164–4165, doi:10.1021/jp010023f.
60. Mulliken, R.S. Electronic Population Analysis on LCAO–MO Molecular Wave Functions. I. *J. Chem. Phys.* **1955**, *23*, 1833–1840, doi:10.1063/1.1740588.
61. Fukui, K.; Yonezawa, T.; Shingu, H. A Molecular Orbital Theory of Reactivity in Aromatic Hydrocarbons. *J. Chem. Phys.* **1952**, *20*, 722–725, doi:10.1063/1.1700523.